NRL Report 6872

Estimating the Diameter of the Plasma in a Propulsion Motor Plume

J. P. WESTON

Applied Physics Branch
Applications Research Division

May 22, 1969

NAVAL RESEARCH LABORATORY
Washington, D.C.

This document has been approved for public release and sale; its distribution is unlimited.

CONTENTS

Abstract	ii
Problem Status	ii
Authorization	ii
INTRODUCTION	1
MICROWAVE BEAM	4
MICROWAVE BEAM ENERGY INTERSECTING A SMALL-DIAMETER PLUME	5
COMPUTED RESULTS	8
DETERMINATION OF ELECTRON DENSITY	11
CONCLUSIONS	15
REFERENCES	19
APPENDIX A — The Volume of Intersection of Two Cylinders Perpendicular to Each Other	20
Table of Symbols as they First Occur	24

ABSTRACT

The diameter of a plasma intersecting the beam of a microwave diagnostic probe must be known to calculate the electron density in the plasma. The ambition to determine the diameter of a small scale model rocket plume by a simple, reliable analysis of the experimental conditions and data obtained by the probe was not completely realized. But some concepts and numbers were developed that have advanced the art of the analysis of the data. The results of an experimental determination of the energy distribution in the microwave beam has been used to calculate the attenuation of this energy by the plasma in an intersecting flame with given attenuation characteristics. The wavelengths of the two microwave beams used were 1.25 cm or 3.0 cm. A method was developed to calculate the attenuation, and a correction factor has been identified to be applied to the apparent attenuation to account for the relative size of the plume when the ratio of the beam diameter to the plume diameter is known.

PROBLEM STATUS

This is an interim report on a continuing problem.

AUTHORIZATION

NRL Problem R07-07
Project RF 17-344-401-4503

Manuscript submitted December 12, 1968.

ESTIMATING THE DIAMETER OF THE PLASMA IN A PROPULSION MOTOR PLUME

INTRODUCTION

In the study of flames and flame plasmas the physical dimensions of the flame plasma are required in determining the electron density and other characteristics of the plasma within definable boundaries. Figure 1 shows a series of photographs of flames fired from the same source but under varied atmospheric pressure conditions. The appearance of the flame is affected not only by the atmospheric pressure but by the exposure time, the depth of focus, and the spectral sensitivity of the film. Figure 2 shows a series of three photographs of the same flame using films which were sensitive to different ranges of the spectrum. This figure also illustrates the difficulty of locating the plasma boundary. The visual effects of the flame apparently mask the plasma region, and some additional or supplemental procedure is needed to determine the actual dimensions of the plasma.

Calculations of the plasma electron density depend on the measured attenuation of a microwave beam per unit of path length through the plasma and on the assumption that the plasma density is macroscopically symmetrical about the axis of the flame (rocket motor plume). This assumption is based on a model of the plume as being subject to turbulent mixing after leaving the exit plane, so that the probability of any characteristic appearing in one section of a ring surrounding the axis of the plume is the same as that

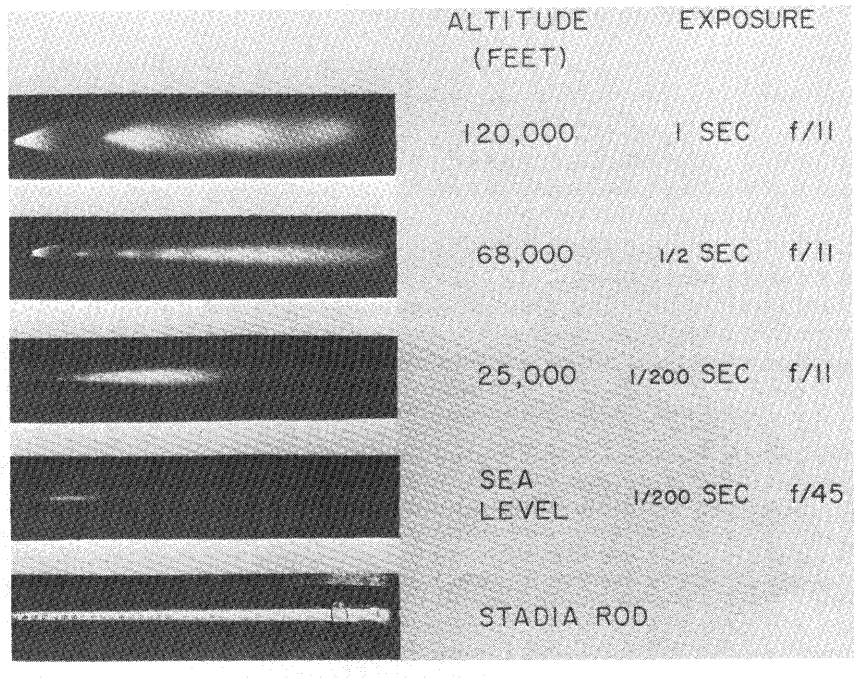

Fig. 1 - Flames under various pressures photographed with the indicated exposure times and depths of focus

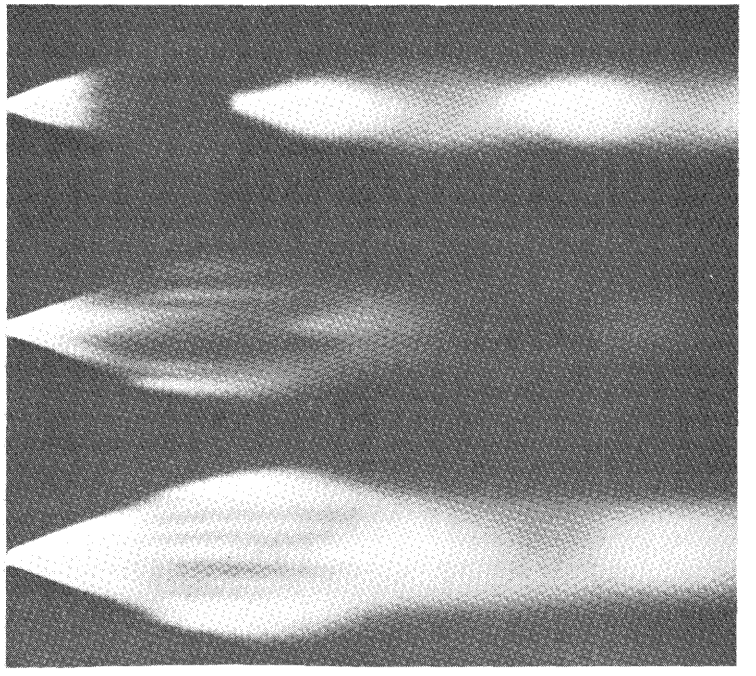

Fig. 2 - A flame as photographed by films with different spectral sensitivities. These photographs show that visual effects do not identify the plasma boundaries.

in any other section of the ring. Consequently the attenuation of the microwave beam is the sum, or integral, of the attenuations in a series of concentric rings along the path through the plume. However, meaningful calculations depend on knowing the diameter of the outer ring of the series or rings forming the plume.

One method of obtaining the plume diameter has been to pass the flame up and down through the microwave beam in a direction perpendicular to both the flame axis and the beam axis as illustrated in Fig. 3 and to measure the distance traveled between the onset and cessation of the attenuation of microwave energy. Another method is to estimate the distance between the two 1/2 maximum attenuation positions about a full maximum position as the flame crosses through the beam and then to use this distance as a criterion for the overall flame diameter. Both methods are used in the laboratory, but both have serious limitations, in particular when the plume seems to be of the same diameter or smaller than the beam it intercepts. In these cases part of the beam energy is not attenuated by the plume and must be considered as a calculable part of the attenuation measurement error.

The NRL flame laboratory altitude chamber is illustrated in Fig. 4 with one of the rocket motors showing between the lenses of the focused antenna assembly. The antennas can be raised or lowered and moved toward or away from the motor, and the motor can be nutated up and down at rates of 2/3, 3, or 10 times per second during firing. The basic instrumentation scheme is diagramed in Fig. 5.

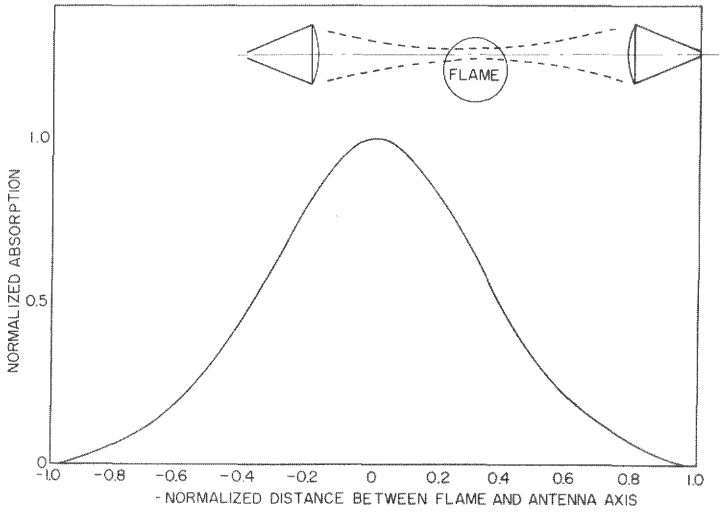

Fig. 3 - Flame attenuation and microwave beam relationship

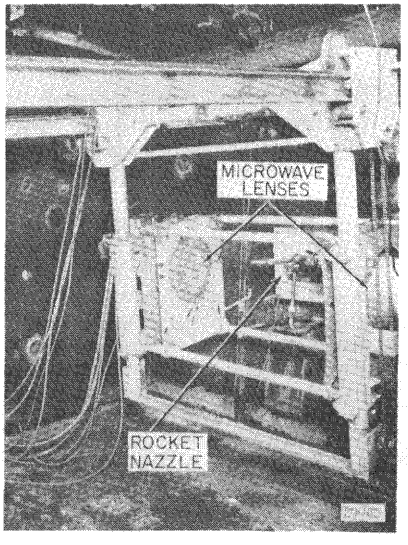

Fig. 4 - Laboratory altitude chamber

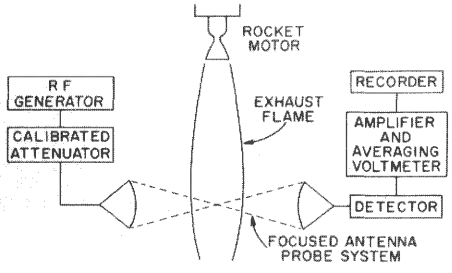

Fig. 5 - Basic instrumentation scheme of the laboratory altitude chamber

MICROWAVE BEAM

The focused microwave beam used in probing the plasma characteristics of the plume will be the starting point of this investigation. In Ref. 1 it was found by theoretical considerations and confirmed experimentally that the electromagnetic energy density is quite nonlinear with respect to the beam radius. In fact the energy density varies as a Bessel function of the first kind and first order such that

$$E = \text{constant} \left[\frac{J_1(z)}{(z)}\right]^2 ,$$

where $z = 2\pi R a_0/\lambda$, in which R is the radius of a chosen point whose energy density is to be calculated, a_0 is the ratio of the lens radius to the lens focal length, and λ is the wavelength of the microwave beam. From $z = 2\pi R a_0/\lambda$ it follows that as R increases from 0, z increases, and E decreases, until at $z = 3.831$, $E = 0$ and $R = 1.52\lambda$, which defines the first minimum energy radius. Let

$$R_1 = \frac{3.831}{2\pi}\frac{\lambda}{a_0} = 0.610\lambda \left[\frac{\text{antenna lens focal length}}{\text{antenna lens radius}}\right] = 1.52\lambda .$$

Further, it was found that the fraction of the radiated energy within the first four successive rings was

$$F_1(E) = 85.9\% ,$$

$$F_2(E) = 5.1\% ,$$

$$F_3(E) = 2.8\% ,$$

and

$$F_4(E) = 1.5\%$$

and within the remaining rings was

$$\sum_{i=5}^{\infty} F_i(E) = 4.7\% .$$

By assuming that the receiving antenna lens receives energy on the identical pattern as the transmitting lens, a rough estimate of the received energy from each ring can be approximated by squaring the amount of energy in each ring, which is proportional to squaring the percentage for each ring:

$$\begin{aligned} \text{received energy} \propto \quad E_i^2 &= E_1^2 + E_2^2 + E_3^2 + E_4^2 + \sum_{i=5}^{\infty} E_i^2 \\ &= 73.7 + 0.26 + 0.078 + 0.022 + \ldots \\ &= 73.7 + 0.36 + \ldots . \end{aligned}$$

Thus the proportion of the energy reaching the receiving antenna from outside the first energy ring is approximately $0.36/73.7 = 4.87\times10^{-3}$ or $\approx 0.5\%$. Hence over 99% of the energy of the beam which reaches the receiver from the focal area comes from within the first minimum energy ring, so that R_1, the radius of the first minimum energy ring,

can also be used as the beam radius. By experiment it was found that over 99% of the energy received at the receiver lens came from an area at the focal distance which was about three wavelengths in diameter for two frequencies tested (at X band, with λ = 3 cm, and at K band, with λ = 1.25 cm). The experimental conditions were such that the lens radius was 6 inches and the focal distance was 15 inches; thus $\alpha_0 = 6/15$. Calculations for the radius yield $R = 0.610\lambda/(6/15) = 1.5\lambda$, so that the diameter is 3.0λ. It appears that the theory verifies the validity of this experimental method. With the assurance that this apparent agreement provided, an attempt was made to measure the energy distribution in the focal area. The curves drawn from the data of the experimental results differed for the two wavelengths, coming closer to the theoretical curve for the shorter wavelength as shown in Figs. 6 and 7. An improved theory (to be published) shows even closer agreement with experimental results. Consequently the experimentally determined values of radiant energy density are used in this development.

MICROWAVE BEAM ENERGY INTERSECTING A SMALL-DIAMETER PLUME

Serious consideration must be given to the energy distribution in the beam when it is used to probe plumes of the same or lesser diameter. Figures 6 and 7 show the energy experimentally measured in Ref. 1 with the beam focused on slots centered on the beam axis with the slot edges increasing in distance from the center to the radius across the focused microwave beams of 3.0 and 1.25 cm wavelength respectively. Both beams were focused on the slots by 12-inch-diameter, 15-inch-focal-length antenna lenses. The curves drawn from the data in Ref. 1 are drawn to a best fit (least squares fit) of the experimental data on the assumption that the rate of change of energy in the expanding slot as a function of the beam radius was a smoothly changing single-valued function.

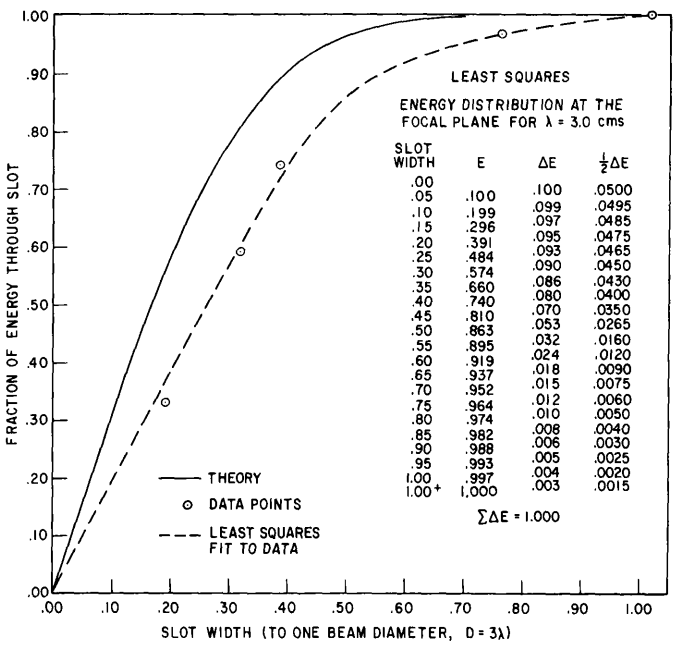

Fig. 6 - Energy distribution within a microwave beam in which λ = 3 cm

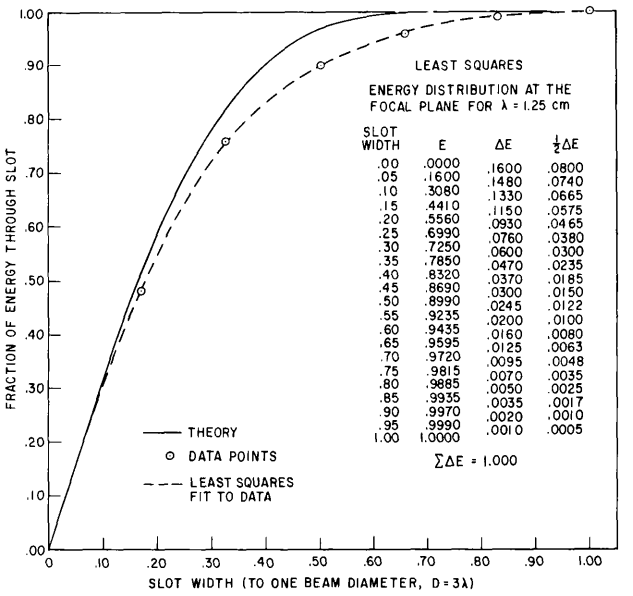

Fig. 7 - Energy distribution within a microwave beam in which $\lambda = 1.25$ cm

The tables in the figures show the fraction of the energy in slot increments over intervals of 5% of the beam radius. The values of $\Delta E/2$ in these tables also give what is referred to as $f(E)_i$, which is the fraction of the total energy in one of the two slabs forming a slot increment. In the derivation that follows, P_t represents all the energy from the transmitter lens into the receiver only when there is no attenuating medium between the lenses. P_r represents all the energy into the receiver whether or not there is some attenuating medium between the lenses. Thus P_t multiplied by $f(E)_i$ is the fraction of that total energy transmitted into the ith slab of the beam, whereas $P_r f(E)_1$ is the fraction of the total received energy which emerges into the receiver lens through that same slab and is represented by the notation P_{ri}. Attenuation by a plume would cause P_{ri} to be less than $P_t f(E)_i$. Figure 8 is an idealized picture of the plume-beam intersection, where a is the distance of the plume axis (r_0) from the beam axis (R_0) and where $P_t f(E)_i$ at a position where the beam intersects the plume is the fraction of energy which passes through a plume cross section $2(\bar{m}_i/2)\Delta z$ and length $2(\bar{\ell}_j/2)$.

The energy transmitted through a uniformly absorbing material is commonly expressed as a decay function, and if we assume that the absorbing medium is of uniform density throughout the plume, then

$$P_{ri} = P_t f(E)_i \, e^{-\gamma \bar{\ell}_j} \tag{1}$$

expresses the energy transmitted through the ith slab, where γ is the absorption constant for the absorbing medium and $\bar{\ell}_j$ is the distance the energy travels through the slab. Taking the $\log_{10}$ of Eq. (1) we get

$$\log_{10} P_{ri} = \log_{10} [P_t f(E)_i] + \log_{10} e^{-\gamma \bar{\ell}_j} \, . \tag{2}$$

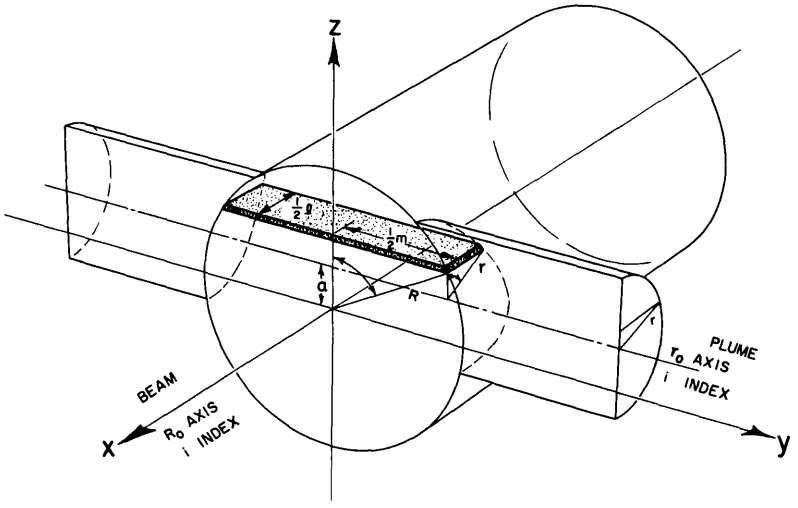

Fig. 8 - Model of the intersection of the plume and the microwave beam. With the beam moving upward through the plume the slabs will be counted off by index numbers which begin at the top in the beam and at the bottom in the plume (at the point where tangency occurred).

But

$$\log_{10} e^{-\gamma \bar{\ell}_j} = -\gamma \bar{\ell}_j \log_{10} e ,$$

and if we define $\gamma \log_{10} e$ as α, where α represents a given attenuation characteristic of the plume, Eq. (1) can be rewritten

$$P_{ri} = P_t f(E)_i \, 10^{-\alpha \bar{\ell}_j}$$

for one slab. To sum up for all the slabs affected,

$$\sum_{i=1}^{n} P_{ri} = P_t \left[f(E)_{i=1} \, 10^{-\alpha \bar{\ell}_{j=n}} + \ldots + f(E)_{i=n} \, 10^{-\alpha \bar{\ell}_{j=1}} \right] . \tag{3}$$

This sum appears as the third term on the right in the equation

$$P_r = P_t - P_t \sum_{i=1}^{n} f(E)_i + \sum_{i=1}^{n} P_{ri} , \tag{4}$$

which applies the conservation of energy concept, and reads: The total received energy equals the total transmitted energy minus the total transmitted energy affected by the plume plus the total energy emerging from the plume. Substituting Eq. (3) into Eq. (4) we get

$$P_r = P_t \left\{ 1 - \sum_{i=1+b}^{n+b} f(E)_i + \left[f(E)_{i=1+b} \left(10^{-a\bar{\ell}_{j=n}} \right) + \ldots + f(E)_{i=n+b} \left(10^{-a\bar{\ell}_{j=1}} \right) \right] \right\}, \quad (5)$$

which can be rewritten to look like an attenuation formula:

$$\log_{10} \frac{P_r}{P_t} = \frac{db}{10} \equiv \log_{10} \left[1 - f(E)_{i=1+b} \left(1 - 10^{-a\bar{\ell}_{j=n}} \right) - \ldots - f(E)_{i=n+b} \left(1 - 10^{-a\bar{\ell}_{j=1}} \right) \right]. \quad (6)$$

The index numbers i, j, n, and b are explained as follows. For example, the indices i for the larger beam and j for the smaller plume are chosen such that the smaller cylinder will have an optimum number of slabs to reach a reasonably accurate approximation of the volume of the intersection. Index number n is the number of slabs in the plume which intercept some part of the beam, which increases in magnitude as the plume moves toward the center, from the top of the beam (external tangent position) to a position where the top of the plume inside the beam is tangent to the top of the beam, and it is a maximum; i is the index of a fraction of beam energy increasing from the top of the beam; j is the index of a slab of plume plasma, increasing from the bottom of the plume; $j_{max} = n$; b is the number of slabs between the top of the plume and the top of the beam and equals zero until the upper boundary of the plume is below the upper boundary of the beam, as the plume moves toward the common center; $b_{max} = (i_{max} - n_{max})/2$.

A matrix for choosing the slabs, which is in the second section of Appendix A, shows that the relationship matching the jth slab to the ith energy fraction is $j = n + b + 1 - i$. The indices are interchanged when the plume is larger than the beam.

COMPUTED RESULTS

The attenuation of the 3.0-cm and the 1.25-cm beams by intersecting plumes were computed for plume sizes varying from 10 times the beam radius to 1/10 the beam radius and for plume plasma attenuation characteristics varying from 300 dB/meter to 0.1 dB/meter. The beam diameter of the $\lambda = 3$ cm beam was determined by experiment to be 10 cm or slightly over 3.3λ. The $\lambda = 1.25$ cm beam diameter was determined to be almost 3.75 cm and chosen to be exactly 3.75 for calculations. Curves were plotted to show the interrelationships, such as the examples of Figs. 9 and 10 showing the attenuation caused by plumes 1/4 the size and 4 times the size respectively of a 3.0-cm-wavelength beam for different α values (plasma densities) as the plume progressively intercepts the beam beginning with edge-to-edge contact and ending at maximum interception with axis-to-axis contact. (In Fig. 8, a varies from $a = R_0 + r_0$, to $a = 0$.) The different symbols in each plot show the variation in the shape of the curves for different values of α; for the case shown in Figs. 9 and 10, namely $\lambda = 3.0$ cm, α describes the attenuation characteristics of the plume as the ratio dB/meter $\equiv 100\alpha$. The computations show that the shape of the curve depends almost entirely on the size of the plume and depends little on the attenuation value except for the higher attenuations.

When the beam is 4 times the radius of the plume ($k = 4$) the plume travels 3 plume radii before reaching the 1/2 maximum attenuation level and 2 more to the maximum level. If the plume continued to travel past the maximum level, it would travel an additional 2 radii to the 1/2 maximum level, so that the width of travel between the two 1/2 maximum points is 4 plume radii or 2 plume diameters. For a beam 1/4 the plume radius ($k = 1/4$) the plume travels about $1/3 \times 5/4 = 5/12$ plume radius to reach a 1/2 maximum attenuation level plus $2/3 \times 5/4 = 10/12$ plume radius to the maximum level, so that the width of travel between the two 1/2 maximum points is about 10/12 plume diameter.

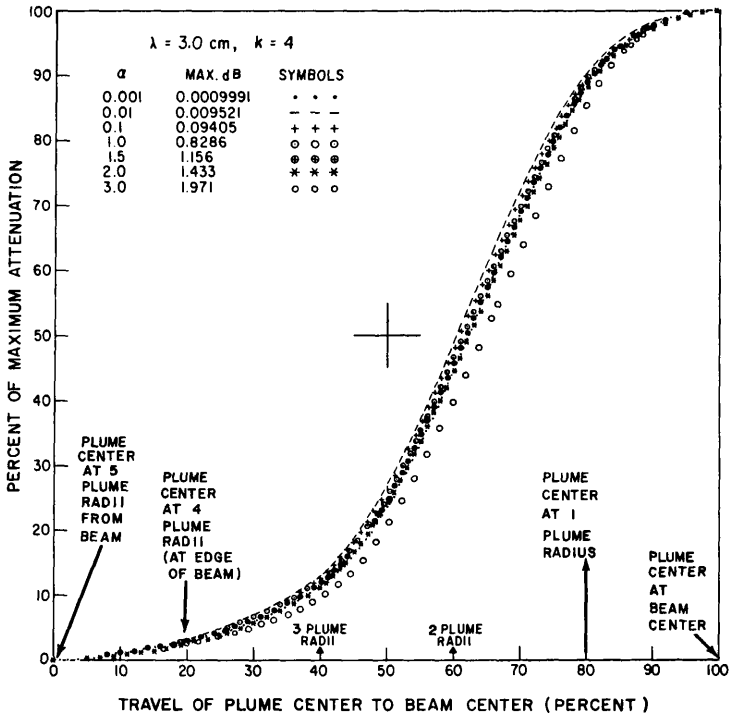

Fig. 9 - Normalized attenuation curve for a λ = 3.0 cm beam 4 times the diameter of the plume

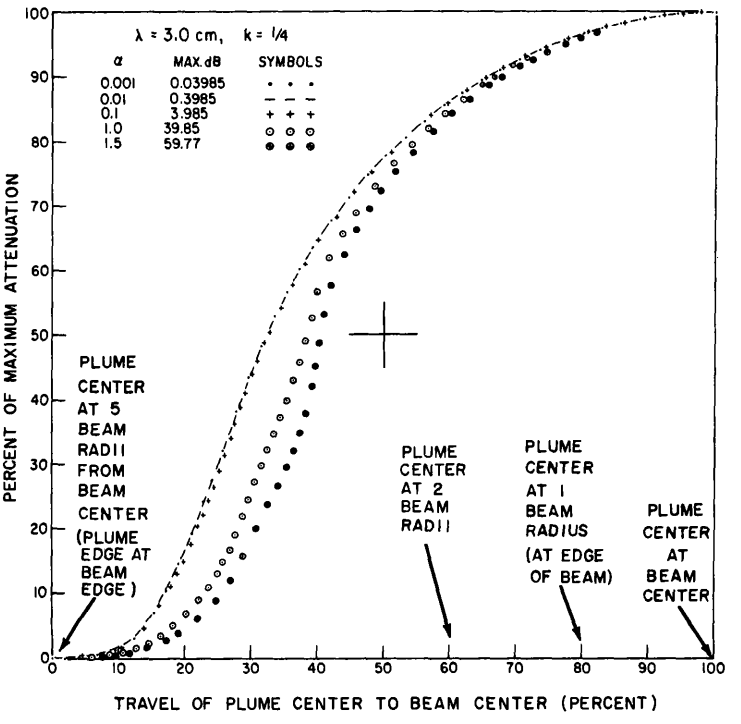

Fig. 10 - Normalized attenuation curve for a λ = 3.0 cm beam 1/4 the diameter of the plume

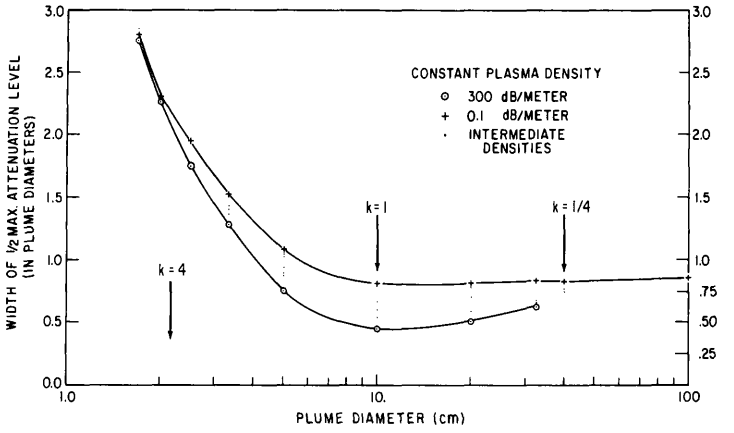

Fig. 11 - Effect of plume diameter on the width of plume travel between the two points of 1/2 maximum attenuation of an X-band microwave beam (λ = 3.0 cm) with a fixed diameter $\approx 3\lambda$ or 9 cm

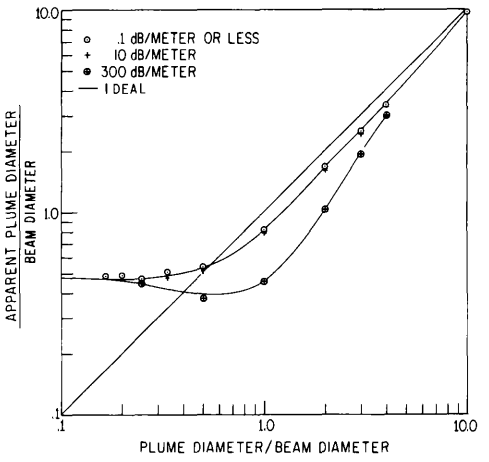

Fig. 12 - Envelope of the apparent plume diameter vs the plume diameter for an X-band (λ = 3.0 cm), normalized by the beam diameter

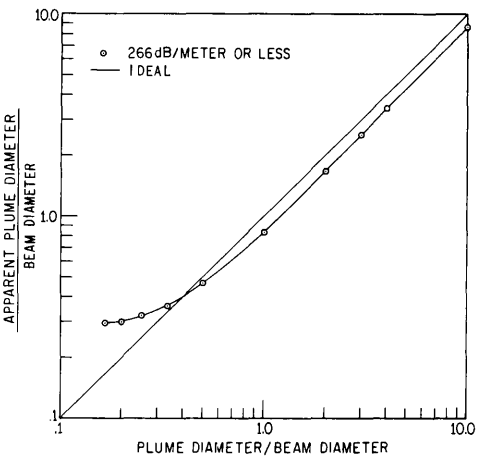

Fig. 13 - Envelope of the apparent plume diameter vs the plume diameter for a K-bank microwave beam (λ = 1.25 cm), normalized by the beam diameter

Figure 11 illustrates the variation with plume size of plume travel between the two points of 1/2 maximum attenuation level and the envelope in which this variation extends as a result of the different plasma densities. The figure shows that the use of the distance between the two 1/2 maximum attenuation points as a criterion for measuring the flame diameter is unreliable as a general method. If it were a good criterion, the plot would be a horizontal line. However, this figure and another version given by Fig. 12 indicates the possibility of estimating the plume size if one is certain that the plume diameter is approximately equal to or is greater than the beam diameter. When the plume diameter becomes a fraction of the beam diameter, the method would fail. Figure 13 is the plot for the 1.25-cm beam corresponding to Fig. 12 for the 3.0-cm beam.

When the plume diameter is known, a correction to the measured attenuation can be calculated by using a plot such as Fig. 14 or 15, which show the values of plume diameter vs maximum attenuation per plume diameter for fixed values of attenuation in dB/meter, for the λ = 3.0 cm and λ = 1.25 cm microwave beams respectively. A plume attenuation correction factor was calculated by taking the ratio of the attenuation of an idealized infinite slab of the same thickness as the plume diameter along the beam and the maximum attenuation of the actual plume. A plot of these correction factors are presented in Fig. 16 for the X-band (3.0-cm) beam and in a different form in Fig. 17 for both the X-band and K-band beams. This correction factor allows one to adjust the measured plume attenuation to the actual attenuation when the plume size is known.

The correction factor was applied in a re-examination of a series of recent experiments. In these experiments the plumes of 20 different propellant types were probed by microwave beams with wavelengths of 3.0 cm, 1.25 cm, and 0.86 cm respectively. The original calculations of the electron density showed a spread which was statistically related to the beam wavelength for each type. When the correction factor was applied to these data, the new calculations of the electron density were essentially in agreement for each propellant type, with no spread evident for different beam wavelengths. The comparison cannot be exact because the microwave beams did not probe the same plumes at the same time. The conditions of the experiment required that only one beam could be used at a time. Thus a separate firing was required for each propellant type as well as for each beam used, and since the conditions of each firing are only approximately the same, the results can be expected to be only approximately the same. Future experiments using two beams simultaneously should result in improved agreement.

DETERMINATION OF ELECTRON DENSITY

The absorption in a uniform plasma is given (2) by

$$\frac{dB}{\text{meter}} = -\,8.686\,\omega\sqrt{\frac{\mu}{2}}\left[-\left(\epsilon_0 - \frac{Ne^2}{m(\omega^2+\nu^2)}\right) + \sqrt{\left(\epsilon_0 - \frac{Ne^2}{m(\omega^2+\nu^2)}\right)^2 + \frac{\nu^2}{\omega^2}\left(\frac{Ne^2}{m(\omega^2+\nu^2)}\right)^2}\right]^{1/2} \tag{7}$$

where the attenuation in dB is seen to be a function of the variable quantities N (the electron density), ω (the electromagnetic frequency in radians/sec), and ν (the electron collision frequency). The constants are the free space magnetic permeability μ, the free space dielectric constant ϵ_0, the electron mass m, and the electron charge e. The equation can be normalized with respect to $f = \omega/2\pi$ and written as

$$\frac{dB}{f} = 2\pi(8.686)\sqrt{\frac{\mu}{2}}\left[-\left(\epsilon_0 - \frac{\frac{N}{f^2}\,\frac{e^2}{m}}{(2\pi)^2 + \frac{\nu^2}{f^2}}\right) + \sqrt{\left(\epsilon_0 - \frac{\frac{N}{f^2}\,\frac{e^2}{m}}{(2\pi)^2 + \frac{\nu^2}{f^2}}\right)^2 + \frac{\nu^2}{(2\pi f)^2}\left(\frac{\frac{N}{f^2}\,\frac{e^2}{m}}{(2\pi)^2 + \frac{\nu^2}{f^2}}\right)^2}\right]^{1/2} \tag{8}$$

The attenuation normalized to frequency, dB/f, was evaluated as a function of $\sqrt{N/f}$, for selected values of ν/f as indicated in the above equation and illustrated in Ref. 2. However the point is not to repeat this effort but to show, in Figs. 18 and 19, the results of computations done for this report when adjusted to show the normalized absorption per meter (dB/f) in relation to plume diameter for constant values of plume attenuation.

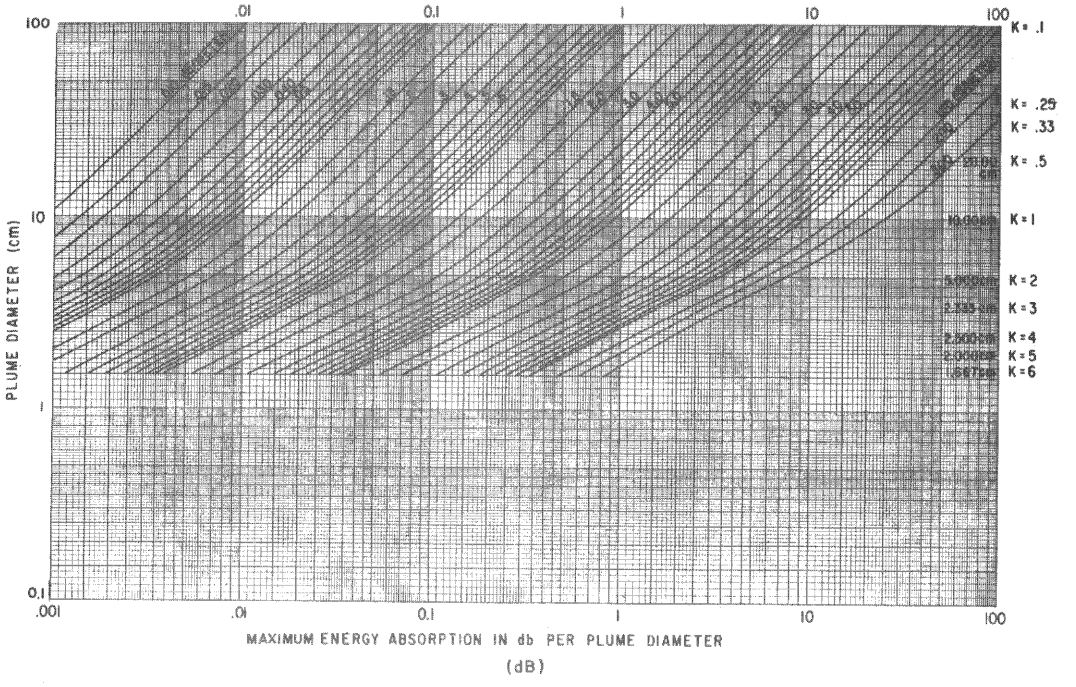

Fig. 14 - Plume diameter vs maximum energy absorption for constant plasma attenuations for $\lambda = 3.0$ cm

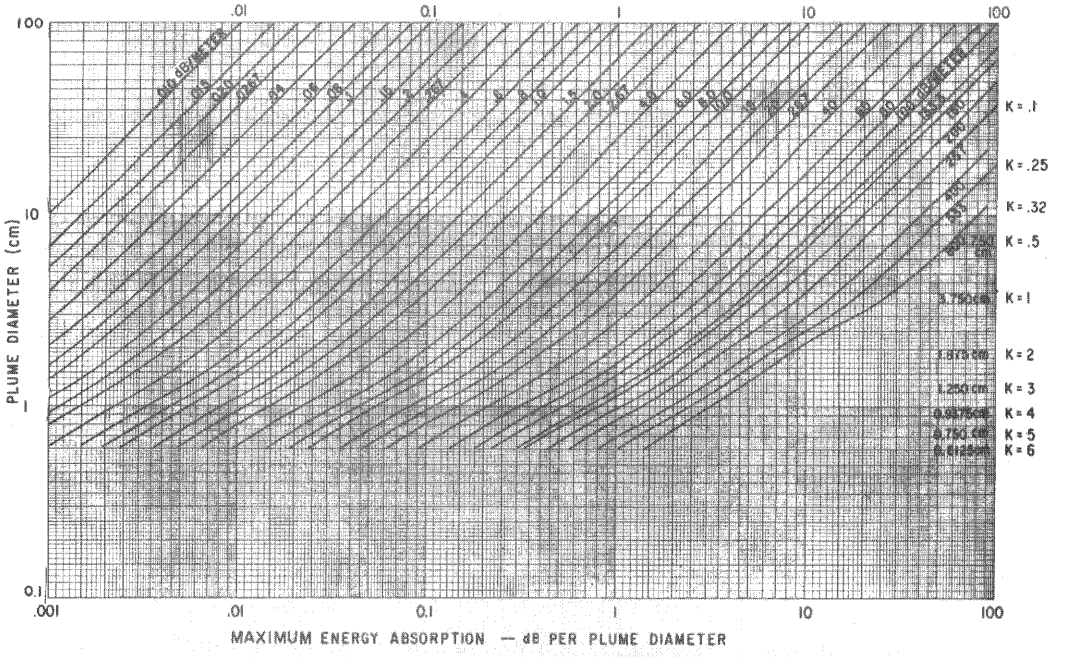

Fig. 15 - Plume diameter vs maximum energy absorption for constant plasma attenuations for $\lambda = 1.25$ cm

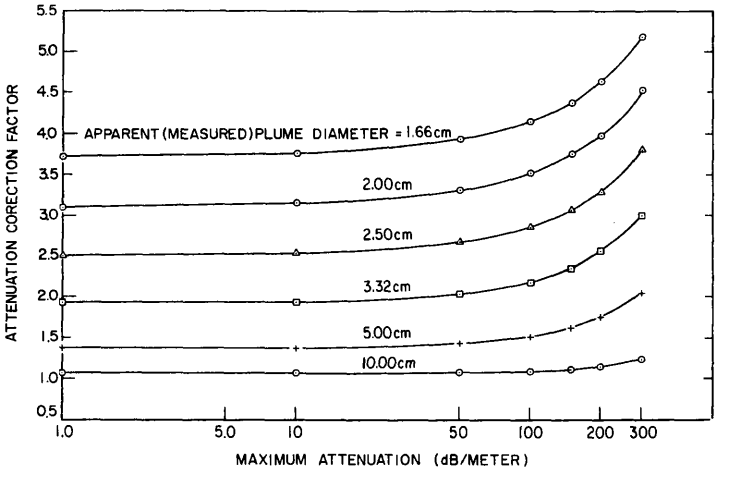

Fig. 16 - Correction factor for the attenuation as a function of the maximum beam attenuation for various measured constant plume diameters and the beam at X band (λ = 3.0 cm)

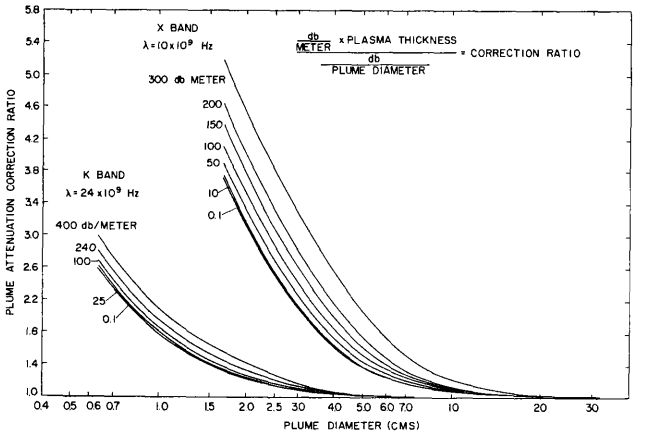

Fig. 17 - Correction factor for the attenuation as a function of the measured plume diameter for various constant plasma densities

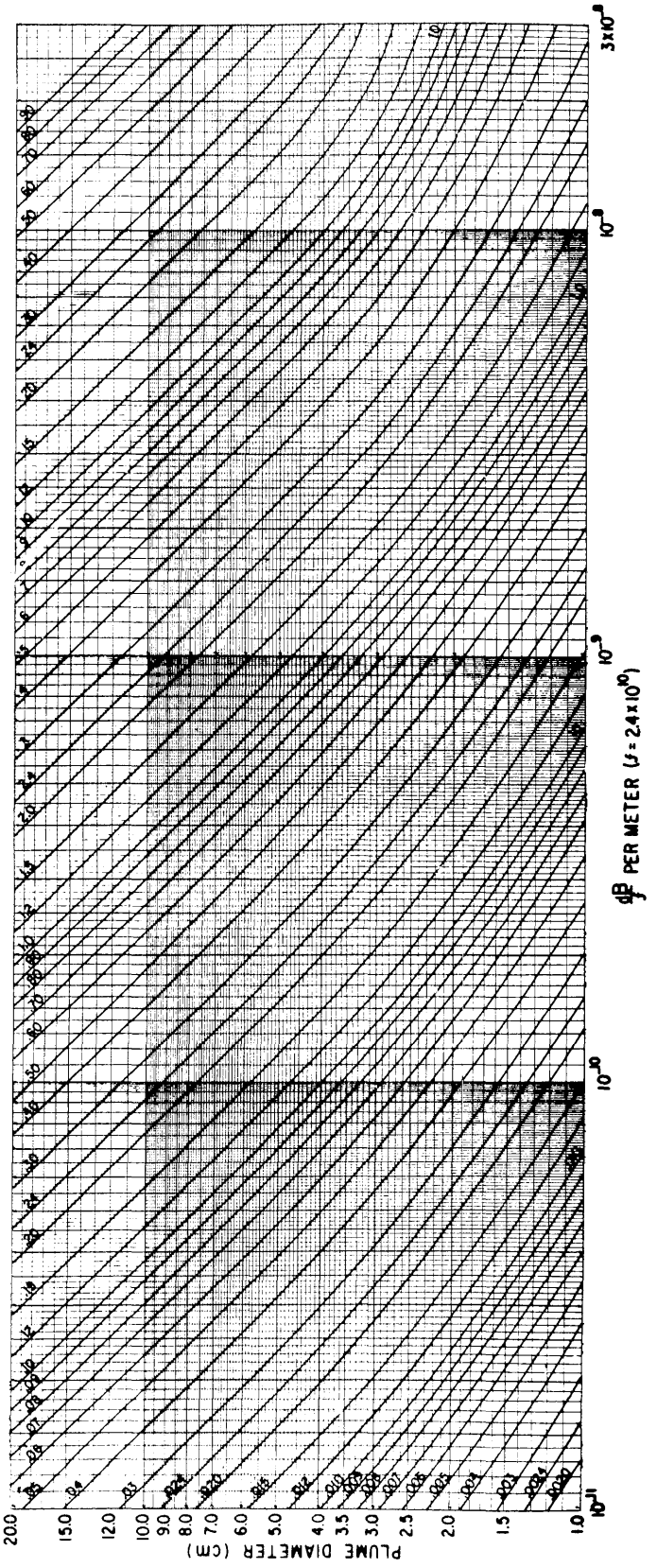

Fig. 19 – Effect of plume diameter on dB/f per meter for constant values of plume attenuation at $f = 2.4 \times 10^{10}$ Hz ($\lambda = 1.25$ cm)

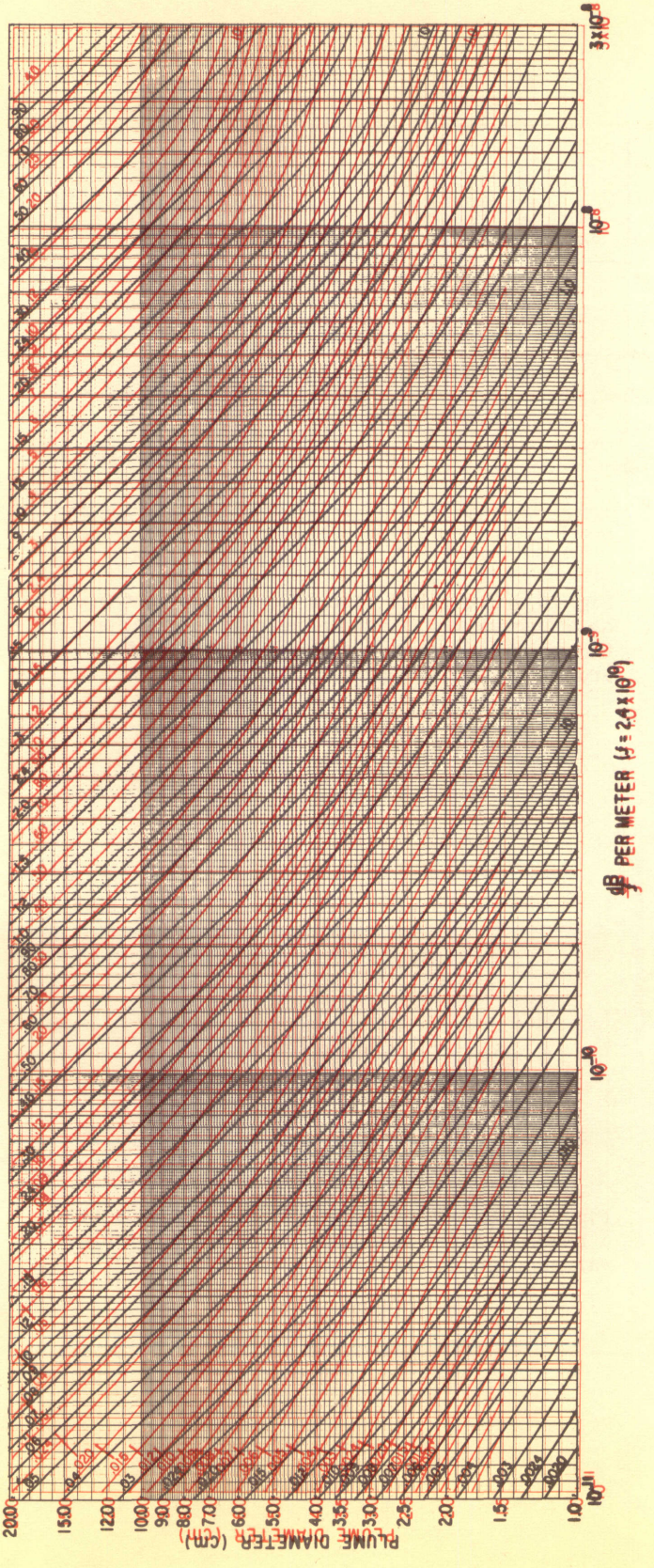

Fig. 18 – Effect of the plume diameter on dB/f per meter for constant values of plume attenuation at $f = 10^{10}$ Hz ($\lambda = 3.0$ cm)

Fig. 19 – Effect of plume diameter on dB/f per meter for constant values of plume attenuation at $f = 2.4 \times 10^{10}$ Hz ($\lambda = 1.25$ cm)

When two or more microwave probes are irradiating the same plume at the same time and in the same region, it follows that they are probing a plasma with one electron density, collision frequency, and plume diameter. Hence the differences in attenuation levels are directly attributable to the differences in wavelength alone. The family of curves illustrated in Fig. 20 show the 3-cm attenuation curves (X band) superimposed upon the 1.25-cm curves (K band) at a fixed electron collision frequency (which is assumed directly proportional to the gas pressure). The representative equation is $\nu \approx 2\times10^{11}\times(P_a/760)$, where the ambient gas pressure P_a is 300 mm Hg. The curves are plotted for plume diameter vs electron density for various values of plume attenuations. Figure 21 shows the same data redrawn for K-band attenuation vs X-band attenuation using constant values of plume diameter and electron density. Since the electron density and plume diameter must be the same regardless of frequency, then the X-band and K-band values must intercept where these values corresponding to each frequency coincide.

Figures 20 and 21 illustrate the theory, but in practice the ambient pressure varies so widely for different experiments that the calculation and plotting of such a set of curves for each pressure condition is impractical. Consequently a modification of the method was required and has been developed.

It became evident while calculating and plotting Fig. 20 that the relative position of the curves in either the X-band family or the K-band family were fixed relative to each other over the entire range of collision frequency, where the resulting $\sqrt{N/f} \leq 10^{-1}$ (Ref. 2). Since the same should be true of any electromagnetic frequency band, the relative position of two superimposed families of curves could be determined by the relative position of a single point on each family of curves derived from all physical conditions being identical except for the two wavelengths. Figure 22 is a graph to be used to calculate the theoretical dB/f for three commonly used microwave beam frequencies as a function of pressure for a single electron density. It has been shown in Ref. 2 that if the values of $\sqrt{N/f}$ remain less than about 10^{-1}, then the logarithmic relationship of dB/f to $\sqrt{N/f}$ remains linear for all values of pressure less than 1 atmosphere; therefore within the limits of $\sqrt{N/f} \leq 10^{-1}$ the curves in Fig. 22 will remain in constant relationship.

The above relationship permits us to find the dB/f for each of the microwave beams, locate them on their respective families of curves such as on Fig. 18 and 19, and then (having one of the figures on a transparency) superimpose the points. Where the lines representing the respective plume attenuations intersect will be the dB/f for their respective beam frequencies (which will yield the same electron density) and the plume diameter.

For example, choose a pressure, say 200 mm Hg from Fig. 22. The X-band dB/f (top curve) for $N = 5.76\times10^{16}/\mathrm{m}^3$ will be 2.15×10^{-9}, and the K-band dB/f for the same N will be 2.57×10^{-10}. Locate the dB/f lines on their respective figures. If one of the figures were a transparency, one could then superimpose the figures. Theoretical curves should give results accurate within the precision of the curves. But the practical results will be sensitive to the lack of precision of the plume attenuation measurements as well, as the uncertainty of the ambient pressure measurement. A figure of merit for the accuracy of this method may well be a figure of wishful thinking if the accuracy of these measurements is not within reasonable limits.

CONCLUSIONS

The initial ambition was to determine the diameter of a small scale-model rocket plume, hopefully by a simple, reliable analysis of the conditions of the experiments and the data obtained by a single microwave probe. This ambition has not been completely

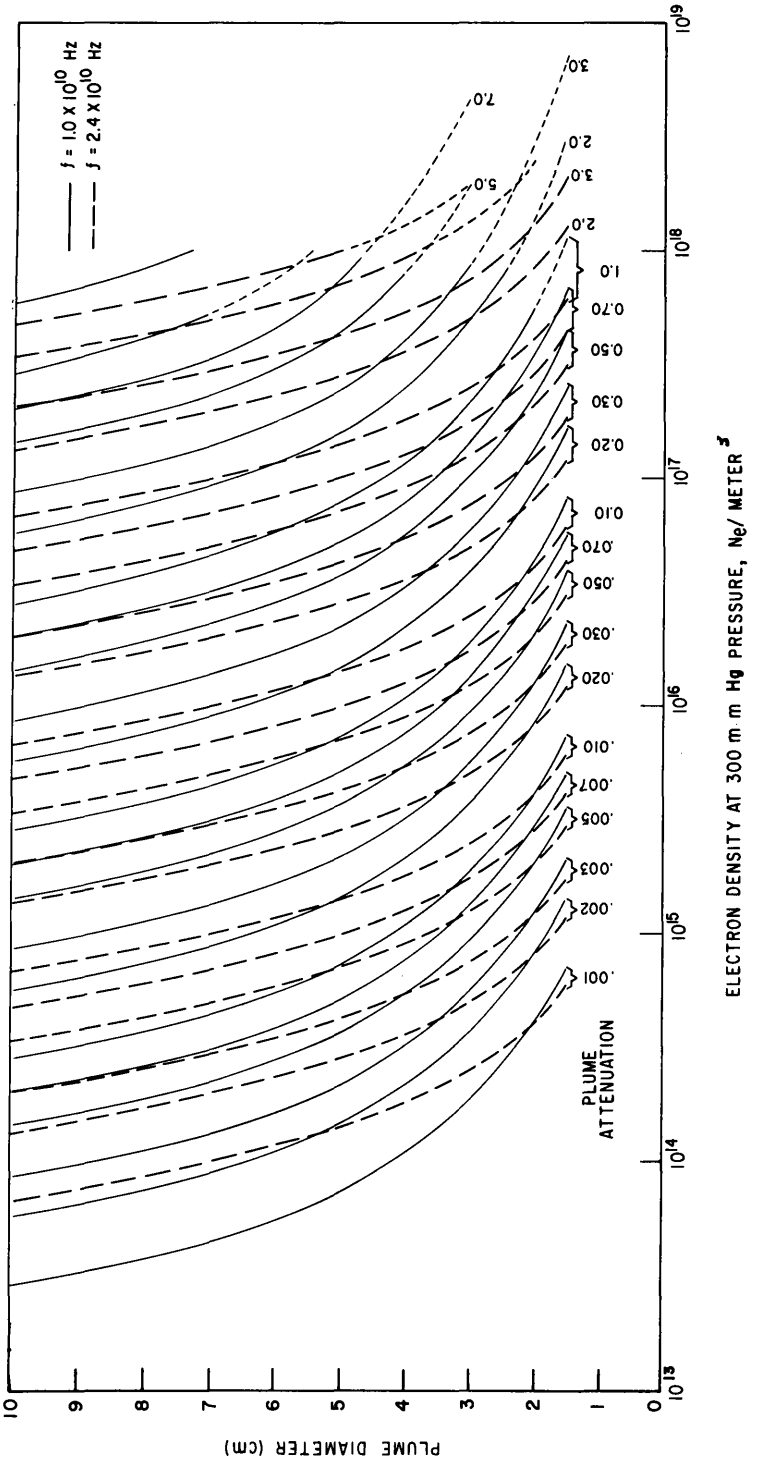

Fig. 20 – Plume diameter and electron density at 300 mm Hg for constant plume attenuation due to the λ = 1.25 cm beam and the λ = 3.0 cm beam

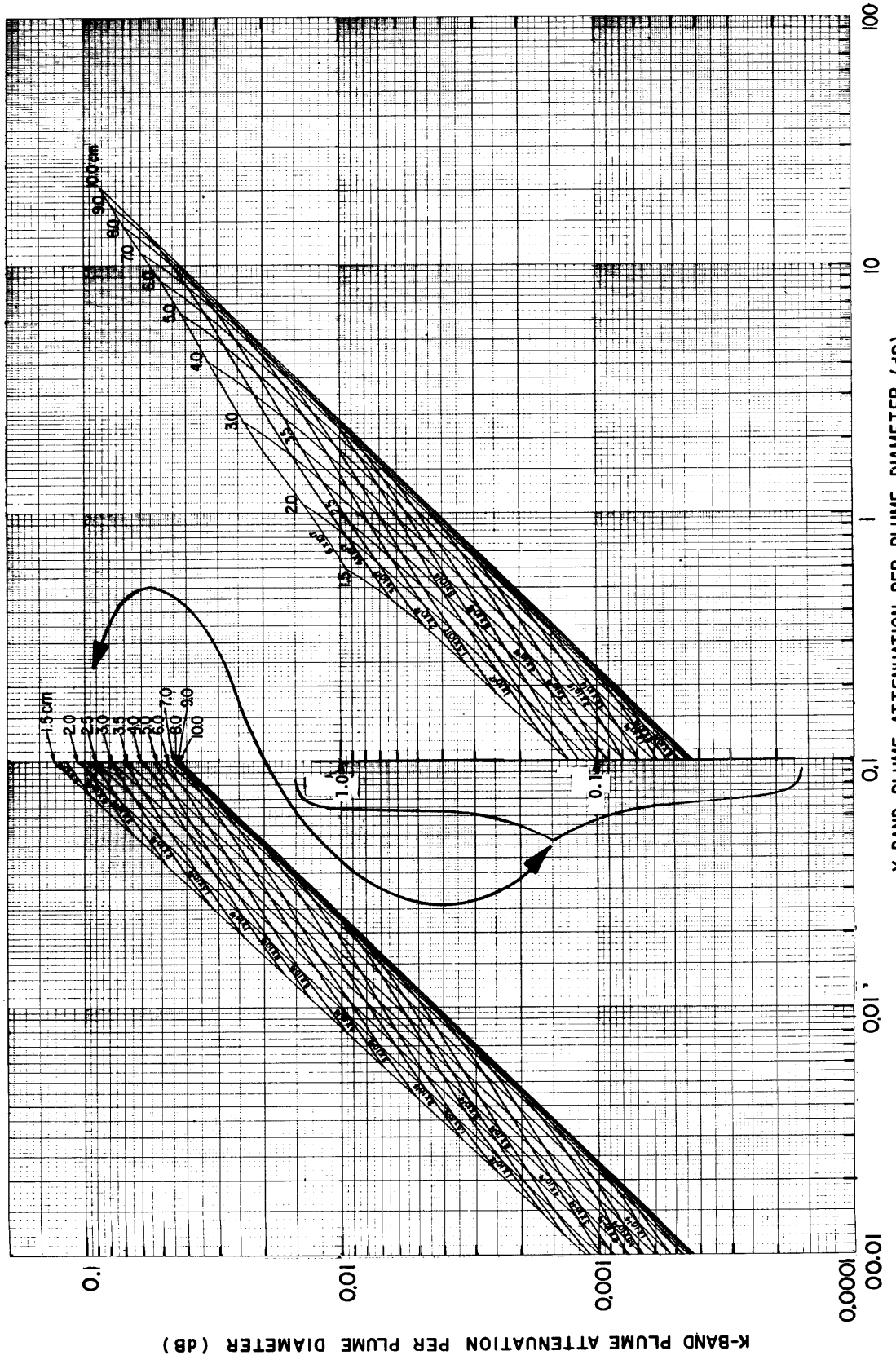

Fig. 21 - K-Band plume attenuation and X-band plume attenuation for constant values of electron density and plume diameter for an ambient pressure of 300 mm Hg

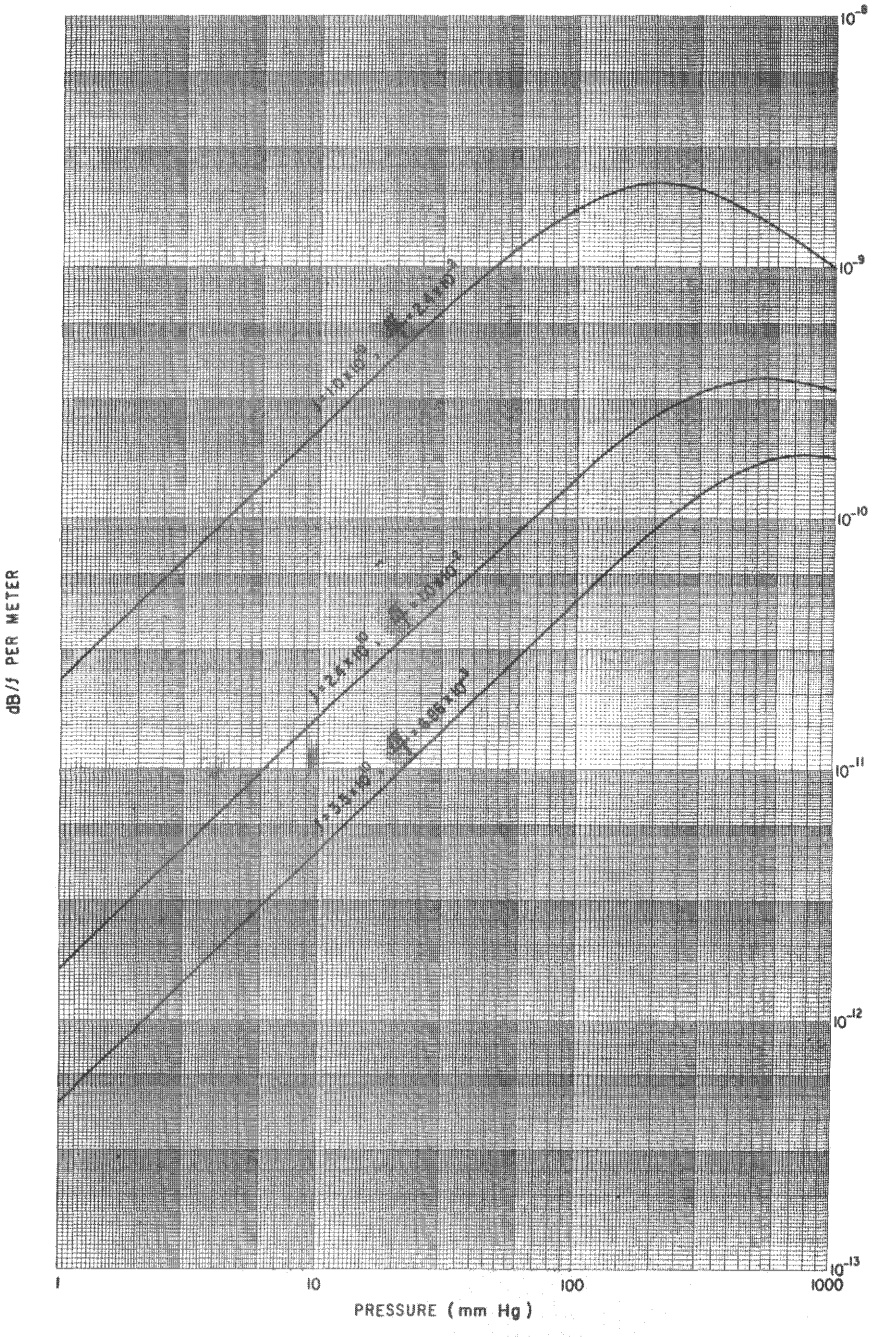

Fig. 22 - Graph to give dB/f per meter as a function of pressure for a constant value of electron density ($5.76 \times 10^{16}/m^3$) and three microwave beam frequencies

realized, but some concepts and some numbers were developed that have advanced the art of analysis of the data. Among the findings were (a) the very limited confirmation of the usefulness of using the 1/2 maximum attenuation level alone, as a criterion for measuring the plume diameter, (b) the positive identification of a correction factor to be applied to the apparent attenuation to account for the relative size of the plume to the beam when the plume size is known, and (c) a method for constructing a graph to aid in determining both the plume size and the attenuation/frequency (dB/f) per meter from the maximum plume attenuation when two frequencies are used simultaneously.

The margin of error in determining the actual plume size and the dB/f per meter, depends mainly on (a) the precision with which the nomograph can be drawn and read and (b) the accuracy of the measurements of the plume attenuations as well as the accuracy of the energy distribution of the beam. However, when the slope and the shape of the curves showing plume attenuation vs k (where k = beam diameter/plume diameter) are considered, the curves seem to be relatively insensitive to the differences in the energy distribution in the beam from the theoretical values, so that perhaps the energy distribution errors are a second-order error source in estimating the accuracy of the graph. This has been assumed, and an uncertainty of $\leq 1/2$ cm in diameter seems quite consistent within our limited experience. A 1-cm plume diameter is less than any we are likely to observe with the size of the present or foreseeable future models, and plumes will probably increase rather than decrease in size, thus making the problem easier. There is some possibility of finding that an estimate of the plume diameter can be made with relatively small degrees of uncertainty (±10%) by measuring the distance traveled by the plume through the beam from onset to cessation of attenuation when the plume diameter is not less than the beam diameter. Perhaps if the distinction between the noise level and the actual attenuation in the recording is clear at 1% of maximum attenuation, an acceptable estimation of the plume diameter can be made. However the ability to distinguish the noise level from such low-level attenuation does not seem possible at the present time.

REFERENCES

1. Rohlfe, D.C., "The Energy Distribution of a Focusing Electromagnetic Probe as used for Near-Zone Measurements," E.E. Thesis, June 8, 1955, George Washington University, Washington, D.C.

2. Balwanz, W.W., "Interactions Between Electromagnetic Waves and Flames, Part 6 — Theoretical Plots of Absorption, Phase Shift, and Reflection, NRL Report 5388, Sept. 23, 1959

Appendix A

THE VOLUME OF INTERSECTION OF TWO CYLINDERS PERPENDICULAR TO EACH OTHER

EXACT VOLUME BY INTEGRATION

As shown in Fig. A1 let the axis of the two cylinders R_0 and r_0 be respectively parallel to the x and y axis with R_0 coincident with the x axis. From Fig. A1,

$$a \equiv |R_0 - r_0| = \text{distance on the } z \text{ axis of } r_0 \text{ from } R_0 \,, \tag{A1}$$

$$dV \equiv \ell m \, dz = \text{volume of a slab in the intersection,} \tag{A2}$$

where

$$m/2 = (R^2 - z^2)^{1/2} \tag{A3}$$

in which R = radius of large cylinder, and

$$\ell/2 = [r^2 - (z - |a|)^2]^{1/2} \,, \tag{A4}$$

in which r = radius of small cylinder. Let $R = kr$; thus $k = R/r$ and

$$R + r = r(k+1) \tag{A5}$$

and

$$0 \leq |a| \leq (R + r) \,. \tag{A6}$$

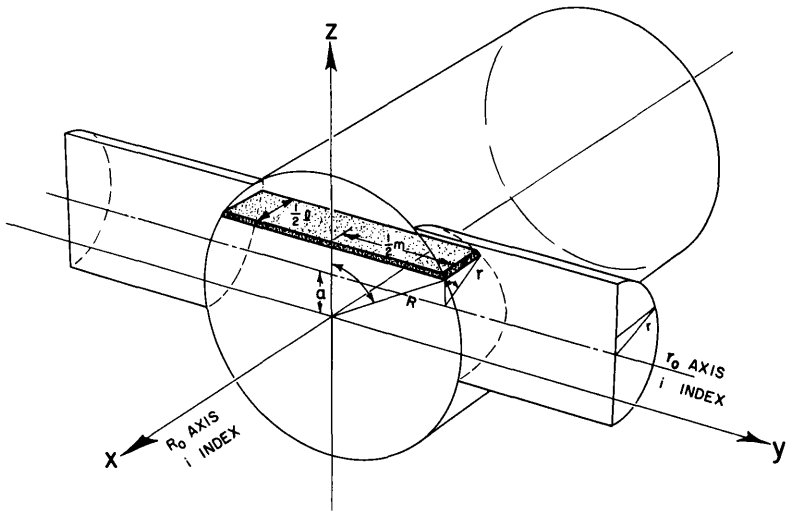

Fig. A1 - Repeat of Fig. 8 but without identifying the beam and plume with the cylinders

The integration limits are

$$-R \le z \le R. \tag{A7}$$

From Eq. (A2) we get

$$dV = 4\ \{(R^2 - z^2)\ [r^2 - (z - |a|)^2]\}^{1/2}\ dz\,, \quad \text{for } \ell \ge 0,\ m \ge 0.$$

or

$$\int dV = 4 \int_0^{a+r} \{(k^2r^2 - z^2)\ [r^2 - (z - |a|)^2]\}^{1/2}\ dz$$

$$+\ 4 \int_0^{a-r} \{(k^2r^2 - z^2)\ [r^2 - (z - |a|)]^2\}^{1/2}\ dz\,, \tag{A8}$$

which turns out to be an elliptic function. The integral is calculated for $0 \le a \le r(k+1)$, where $k = 1, 2, 3, 4, 5, 6$, and the values are illustrated in Fig. A2 as a function of V/kr^3 (which is a constant called the coefficient of volume) vs a/r.

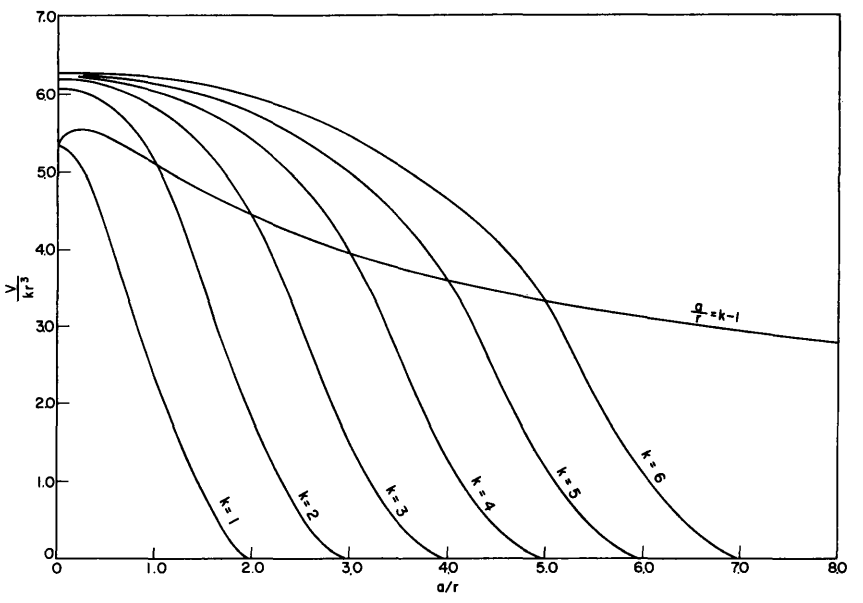

Fig. A2 - Values for the volume of intersection as given by Eq. (A8)

APPROXIMATE VOLUME BY SUMMATION OF SLABS

To approximate the volume of intersection we can divide the intersection of the two cylinders into a series of parallel slabs with a normalized cross-sectional area, say

$$A_i/2 = \frac{1}{R^2} \int_{z_{i-1}}^{z_i} \sqrt{R^2 - z_i^2 \; \Delta z} \; ,$$

where z_i is distance from the axis R_0, and where the length of a slab surface will be a normalized length $\ell_j = 1/r \sqrt{r^2 - z_j^2}$, in which z_j is the distance from the axis r_0. Since Δz is the same in both cylinders, then $R/\Delta z = p/2$, where p is the number of slabs across the diameter of the large cylinder. Thus $i = 0, 1, 2, \ldots, p$. Then $z_i = |(p/2) - i| \Delta z$. Similarly $z_j = |(q/2) - j| \; \Delta z$, where $r/\Delta z = q/2$ and $j = q, q-1, \ldots, 1$. When the two cylinders are tangent, $i = j = 0$. The physical scheme is illustrated in Figs. A3 and A4. The resultant volume is expressed in the following equation, in which A_i is a cross-sectional area and $\bar{\ell}_j = (\ell_j + \ell_{j-1})/2$:

$$V = \sum_{i=1+b}^{n+b} A_i \bar{\ell}_j \; , \tag{A9}$$

where $j = n + b + 1 - i$, n is the number of slabs in the intersection ($n_{max} = q$), and b is the number of area increments in the larger cylinder between the top of the smaller cylinder and the top of the larger one as the smaller cylinder moves toward the center of the larger (always counting from the initial point of tangency), $b = 0$ when $i_{max} \leq q$. $1 \leq b \leq (p - q)/2$ when $q = i_{max} \leq (p + q)/2$. When $i_{max} = (p + q)/2$, the axis of the two cylinders R_0 and r_0 are crossing, and in Eq. (A1), $a = (R_0 - r_0) = 0$.

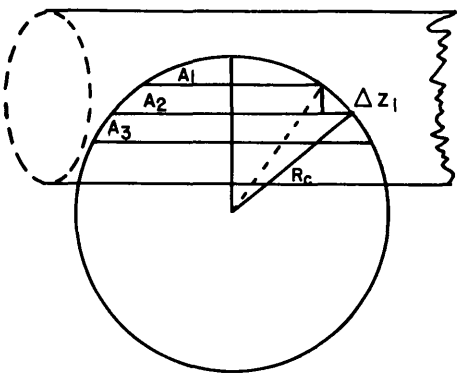

Fig. A3 - Cross section of the microwave beam

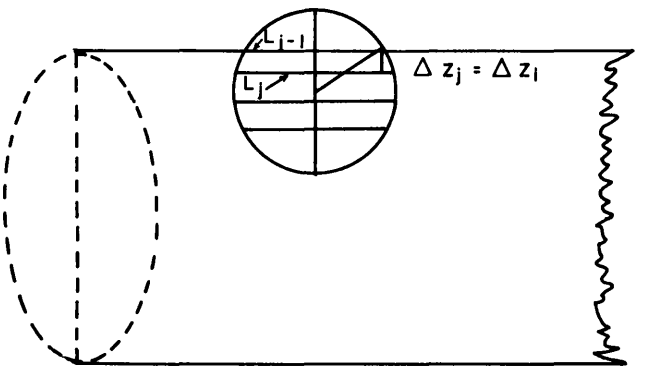

Fig. A4 - Cross section of the flame

The matrix in Fig. A5 illustrates the summation scheme described in Eq. (A9) for successive volumes of intersection starting from the point of tangency, where $2R/\Delta z = p = 12$ and $2r/\Delta z = q = 8$. As indicated by the example at the bottom of the figure,

$$V_0 = A_0 \bar{\ell}_0 = 0 \; , \qquad n = 0 \; ,$$
$$V_1 = A_1 \bar{\ell}_1 \; , \qquad n = 1 \; ,$$
$$V_2 = A_1 \bar{\ell}_2 + A_2 \bar{\ell}_1 \; , \qquad n = 2 \; ,$$
$$V_3 = A_1 \bar{\ell}_3 + A_2 \bar{\ell}_2 + A_3 \bar{\ell}_1 \; , \qquad n = 3 \; ,$$

etc.

	A_1	A_2	A_3	A_4	A_5	A_6	A_7	A_8	A_9	A_{10}	A_{11}	A_{12}
ℓ_1	$A_1\ell_1$	$A_2\bar{\ell}_1$						$A_8\bar{\ell}_1$		$A_{10}\bar{\ell}_1$		
ℓ_2	$A_1\bar{\ell}_2$						$A_7\bar{\ell}_2$		$A_9\bar{\ell}_2$			
ℓ_3						$A_6\bar{\ell}_3$		$A_8\bar{\ell}_3$				
ℓ_4					$A_5\bar{\ell}_4$		$A_7\bar{\ell}_4$					
ℓ_5				$A_4\bar{\ell}_5$		$A_6\bar{\ell}_5$						
ℓ_6			$A_3\bar{\ell}_6$		$A_5\bar{\ell}_6$							
ℓ_7		$A_2\bar{\ell}_7$		$A_4\bar{\ell}_7$								
ℓ_8	$A_1\bar{\ell}_8$ b = 0	b = 1	$A_3\bar{\ell}_8$ b = 2	b = 3	b = 4							

FOR EXEMPLE: $V_{10} = \sum_{i=1+b}^{n+b} A_i\ell_j = \sum_{3}^{10} A_i\ell_j$, $n = q = 8$, $b = 2$, $j = n + b + 1 - i$

Fig. A5 - Summation scheme of Eq. (A9)

When Δz is small compared to the radius, the relative curvature of the cylindrical boundaries approach the character of flat surfaces. Thus the volume of the region bounded by A_i, the cylinder walls, and the planes containing ℓ_j and ℓ_{j-1} approach the volume of a truncated prism except for the end sections, where $A_1\ell_1 = A_p\ell_q$ are like pyramids and $\Delta v_1 = A\ell_1/3$. The sections $A_1\ell_q = A_p\ell_1$ are like simple prisms and can be included in the general formula

$$V_{ij} = A_i[\ell_j + (1/2)(\ell_{j-1} - \ell_j)] = (1/2)A_i(\ell_j + \ell_{j-1}) \ .$$

Table of Symbols as They First Occur

Symbol	Definition	Page
E	Electromagnetic Energy Density	4
$J_i(Z)$	Discriminant of Bessel Function	4
λ	Electromagnetic Wavelength	4
α_0	Ratio of Lens Radius/Lens Focal Length	4
R	Radius of First Minimum Energy Ring = Beam Radius	4
P_r	Energy Received through Receiver Lens	6
P_t	Energy Received without Plume Interference	6
$f(E)_i$	Fraction of Energy Impinging on the ith Slab of Beam	6
ℓ_j	Distance Energy Travels through the Plume in the ith Slab	6
R_0	Beam Axis of Large Cylinder	6
R	Beam Radius	7
r_0	Plume Axis	6
r	Plume Radius	7
k	Ratio R/r	8
γ	Arbitrary Absorption Constant	6
n	Total Number of Plume Slabs Interacting with the Beam	8
i	Index Number of Slab Corresponding to its Position in the Beam	8
j	Index Number of Slab Corresponding to its Position in the Plume	8
p	Number of Slabs in Large Cylinder	22
q	Number of Slabs in Small Cylinder	22
ω	Electromagnetic Frequency in Radians/Sec = $2\pi f$	11
f	Electromagnetic Frequency in Cycles/Sec or Hertz	11
ν	Electron Collision Frequency in Collisions/Sec	11
ϵ_0	Free Space Dielectric Constant	11
μ	Free Space Magnetic Permeability	11
N	Electron Number Density	11
e	Electron Charge	11
m	Electron Mass	11
P_a	Ambient Pressure of Gases in the Plume	16

Security Classification

DOCUMENT CONTROL DATA - R & D

(Security classification of title, body of abstract and indexing annotation must be entered when the overall report is classified)

1. ORIGINATING ACTIVITY *(Corporate author)*

Naval Research Laboratory
Washington, D.C. 20390

2a. REPORT SECURITY CLASSIFICATION

Unclassified

2b. GROUP

3. REPORT TITLE

ESTIMATING THE DIAMETER OF THE PLASMA IN A PROPULSION MOTOR PLUME

4. DESCRIPTIVE NOTES *(Type of report and inclusive dates)*

An interim report on a continuing problem.

5. AUTHOR(S) *(First name, middle initial, last name)*

J.P. Weston

6. REPORT DATE

May 22, 1969

7a. TOTAL NO. OF PAGES

28

7b. NO. OF REFS

2

8a. CONTRACT OR GRANT NO.

NRL Problem R07-07

b. PROJECT NO.

RF 17-344-401-4503

c.

d.

9a. ORIGINATOR'S REPORT NUMBER(S)

NRL Report 6872

9b. OTHER REPORT NO(S) *(Any other numbers that may be assigned this report)*

10. DISTRIBUTION STATEMENT

This document has been approved for public release and sale; its distribution is unlimited.

11. SUPPLEMENTARY NOTES

12. SPONSORING MILITARY ACTIVITY

Department of the Navy
(Office of Naval Research),
Washington, D.C. 20360

13. ABSTRACT

The diameter of a plasma intersecting the beam of a microwave diagnostic probe must be known to calculate the electron density in the plasma. The ambition to determine the diameter of a small scale model rocket plume by a simple, reliable analysis of the experimental conditions and data obtained by the probe was not completely realized. But some concepts and numbers were developed that have advanced the art of the analysis of the data. The results of an experimental determination of the energy distribution in the microwave beam has been used to calculate the attenuation of this energy by the plasma in an intersecting flame with given attenuation characteristics. The wavelengths of the two microwave beams used were 1.25 cm or 3.0 cm. A method was developed to calculate the attenuation, and a correction factor has been identified to be applied to the apparent attenuation to account for the relative size of the plume when the ratio of the beam diameter to the plume diameter is known.

DD FORM 1 NOV 65 1473 (PAGE 1)

S/N 0101-807-6801

Security Classification

Security Classification

14. KEY WORDS	LINK A ROLE	LINK A WT	LINK B ROLE	LINK B WT	LINK C ROLE	LINK C WT
Plumes						
Rocket exhaust						
Dimensions						
Measurements						
Microwave equipment						
Electron density (concentration)						
Exhaust flames						
Plasmas (physics)						
Thickness						
Estimates						
Probes						
Microwave frequencies						

DD FORM 1 NOV 65 1473 (BACK)
(PAGE 2)

Security Classification